Strong Ground Motion Prediction of Future Large Earthquake from Niavaran Fault in Tehran, Iran by Finite Fault Method

M. Samaei & M. Miyajima
Kanazawa University, Japan

M. Tsurugi
Geo-Research Institute, Japan

A. Fallahi
Azarbaijan University of Tarbiat Moallem, Iran

SUMMARY:
Tehran, the capital of Iran is surrounded by many active faults; these active faults have caused major earthquakes that have completely destructed the ancient city of Rey in the past. Therefore evaluation of severity of future large earthquake in this city is necessary. In this study Niavaran Fault which located in North of Tehran is chosen as target fault. New researches show that there are more evidences for activity of this fault compared to North Tehran Fault, the other major fault in Northern Tehran (Abbassi and Farbod, 2009). Finite fault modeling method has adopted here to generate acceleration time histories at 836 points in metropolitan of Tehran to draw PHA shake map of Tehran for generic rock sites. "Recipe for Predicting Strong Ground Motions from Future Large Earthquakes" of Irikura et al (2004) and Irikura and Miyake (2010) is followed to characterize source model of Niavarn Fault. PHA from simulations varies from 100 cm/sec^2 in Southern parts of the city to 800 cm/sec^2 for Northern parts. A comparison of results of simulations in different distances also has been made with three attenuation relationships which have developed for Iranian plateau.

Keywords: Strong Ground Motion Prediction, Finite Fault, Tehran, Niavaran Fault, Recipe

1. INTRODUCTION

Tehran, the capital of Iran with the population of over 10 million people is surrounded by many active faults (Tchalenko et al, 1974; Berberian et al, 1983). This city was built after the last destructive earthquake that devastated the ancient city of Rey in 1177 A.D. (Mw≈7.2) which is now a suburb of south Tehran. The 1177 A.D. earthquake is not the only earthquake that has occurred in Tehran with magnitude bigger than 7 but this city has been stricken by other major earthquakes before that (Berberian et al, 1983; Berberian and Yeats, 1999). Existence of active faults and destructive historical earthquakes indicate the necessity of the evaluation of the severity of earthquake occurrence in this city.

Niavaran fault is a left lateral strike-slip fault located in north of Tehran. This fault was believed to have a total length of 13 kilometres (Berberian et al, 1983) and therefore incapable of causing large earthquakes but new researches (Abbassi and Farbod, 2009) show that the length of this fault is about 45 kilometres so the historical earthquakes in north Tehran can be caused by this fault rather than North Tehran fault. Location of the Niavaran Fault is shown in **Figure 1.** Evidences show that the left

In this study we adopt finite fault method (Beresnev and Atkinson, 1997; Motazedian and Atkinson, 2005; Boore, 2009) to produce acceleration time histories at over 800 points in metropolitan of Tehran to provide a shake map of peak horizontal acceleration (PHA) in the city. The target fault will be Niavaran Fault. For source model characterization we follow recipe for predicting strong ground motion from crustal earthquake scenarios (Irikura et al, 2004; Irikura and Miyake, 2010). At the end we compare results of this study with some attenuation relations that have developed for Iranian plateau.

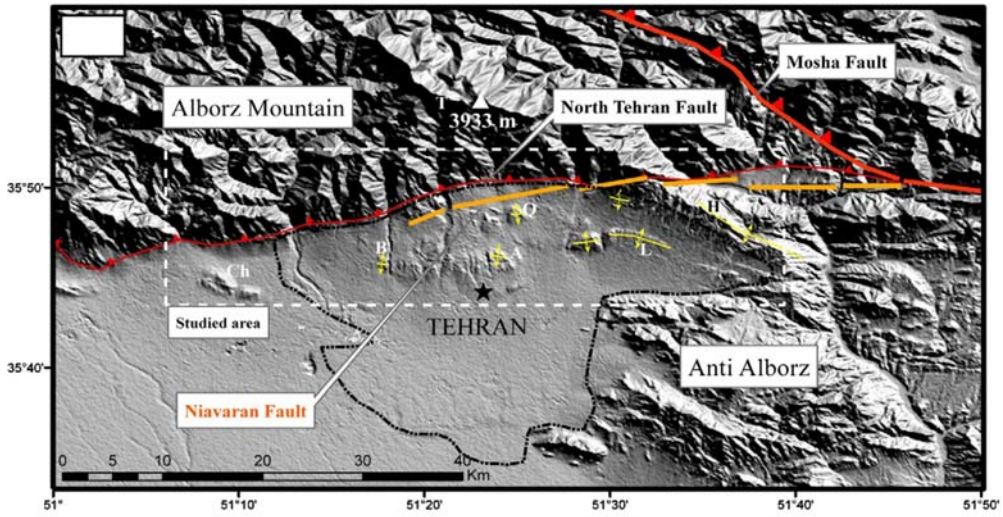

Figure 1. Location on Niavaran Fault and Tehran metropolitan (after Abbassi and Farbod 2009)

2. FINITE FAULT MODELING

One of the most useful methods to simulate ground motion for a large earthquake is based on the simulation of several small earthquakes as subevents that comprise a large fault-rupture event. This idea for the first time was introduces by Hartzell (1978); when he used this method to model the El Centro displacement record for the 1940 Imperial Valley earthquake. In this method a large fault is divided into N subfaults and each subfault is considered as a small point source. The contributions of all point sources are summed in the observation point and large event is produced.

One of the simple solutions for this method was proposed by Beresnev and Atkinson (1997). In this solution target fault is divided to $nl \times nw$ ($=N$) subfaults with unique dimensions. For each subfault ground motion is being produced by stochastic source point method with an ω^2 model. By considering the effects of path and site, the produced motions for all subfaults are summed in the observation point with a proper time delay to obtain the ground motion acceleration from the entire fault:

$$a(t) = \sum_{i=1}^{nl} \sum_{j=1}^{nw} a_{ij}\left(t + \Delta t_{ij}\right) \tag{2.1}$$

where Δt_{ij} is relative delay time for the radiated wave from the ijth subfault to reach the observation point and a_{ij} is the subevent (motion) which coincides with the ijth subfault. Each $a_{ij}(t)$ is calculated by the stochastic point-source method of Boore (1983;2003). In Boore's method the acceleration spectrum for a subfault at a distance R_{ij} is modeled as a point source with an ω^2 shape. The acceleration spectrum of shear wave of the ijth subfault, $A_{ij}(f)$, is described by:

$$A_{ij}(f) = CM_{0ij} \frac{(2\pi f)^2}{\left[1+\left(\frac{f}{f_{0ij}}\right)^2\right]} \frac{e^{\frac{-\pi f R_{ij}}{Q(f)\beta}}}{R_{ij}} D(f) e^{-\pi f \kappa_0} \tag{2.2}$$

where M_{0ij}, f_{0ij}, and R_{ij} are the ijth subfault seismic moment, corner frequency, and distance from the observation point, respectively. The constant $C=\mathcal{R}^{\theta\varphi}4FV/(4\pi\rho\beta^3)$, where $\mathcal{R}^{\theta\varphi}$ is radiation pattern (average value of 0.55 for shear waves), F is free surface amplification (2.0), V is partition onto two horizontal components (0.71), ρ is density, and β is shear wave velocity. f_{0ij} is the corner frequency of the ijth subfault. $D(f)$ is the site amplification and the term $\exp(-\pi f \kappa_0)$ is a high-cut filter to model near surface κ_0 effects. The quality factor, $Q(f)$, is inversely related to anelastic attenuation. The implied $1/R$ geometric attenuation term is applicable for body-wave spreading in a whole space.

Despite all advantages of the presented approach by Beresnev and Atkinson (1997), Motazedian and Atkinson (2005) showed that the received energy at the observation point is very sensitive to subfault sizes e.g. as the subfault sizes are increased, the energy at low frequency is decreased and the energy at high frequencies is increased. They overcame this problem by introducing a "dynamic corner frequency". In their model, the corner frequency is a function of time, and the rupture history controls the frequency content of the simulated time series of each subfault. The rupture begins with a high corner frequency and progresses to lower corner frequencies as the ruptured area grows.

In Motazedian and Atkinson's program (EXSIM), the acceleration spectrum of the shear wave of the *ij*th subfault, $A_{ij}(f)$, is described by

$$A_{ij}(f) = CM_{0ij}H_{ij}\frac{(2\pi f)^2}{\left[1+\left(\frac{f}{f_{0ij}(t)}\right)^2\right]}\frac{e^{\frac{-\pi f R_{ij}}{Q(f)\beta}}}{R_{ij}}D(f)e^{-\pi f\kappa_0} \tag{2.3}$$

where the dynamic corner frequency, $f_{0ij}(t)$, is defined as a function of the cumulative number of ruptured subfaults, $N_R(t)$, at time t:

$$f_{0ij}(t) = 4.9\times 10^6 \beta N_R^{-1/3} N^{1/3}\left(\frac{\Delta\sigma}{M}\right)^{1/3} \tag{2.4}$$

H_{ij} is a scaling factor for conserving the total area under the spectrum of subfaults as the corner frequency decreases with time which is:

$$H_{ij} = \left(N\sum\left\{\frac{f^2}{\left[1+\left(\frac{f}{f_0}\right)^2\right]}\right\}^2 \Big/ \sum\left\{\frac{f^2}{\left[1+\left(\frac{f}{f_{0ij}}\right)^2\right]}\right\}^2\right)^{1/2} \tag{2.5}$$

Boore (2009) also made some modifications on the code of finite fault modeling (EXSIM) so it can have better agreement in producing motions with point source modeling (SMSIM, Boore 2005).

Modified version of the program EXSIM has adopted here for simulation of earthquake ground motion from rupture of Niavaran fault in Metropolitan of Tehran.

3. ANALYSIS AND RESULTS

As it pointed before, the target fault for our simulation is Niavaran fault. The location, geometry and mechanism of the fault are based on the work of Abbassi and Farbod (2009). The dip of this fault is 50 degrees towards north. The upper depth and lower depth are decided from recorded events (with M>2.5) of Institute of Geophysics, University of Tehran (IGTU) and also International Institute of Earthquake Engineering and Seismology (IIEES) from 1998 to 2011. All the recorded events have the hypocenteral depth between 3 to 18 kilometers so the siesmogenic depth decided to be from 3 to 18 kilometers.

In finite fault method, modeling of the finite source requires the orientation and dimensions of the fault plane, the dimensions of subfaults and the location of the hypocenter. The parameters used in this study are listed in **Table 1**. Moment magnitude is calculated from empirical relationships of Wells and Coppersmith (1994) for strike-slip faults by considering rupture area. Q value, geometric spreading, high cut filter and percentage of pulsing area, are based on the work by Motazedian (2006) for earthquakes in northern Iran. Stress parameter of 120 bars is chosen instead of 68 bars from Motazedian (2006) because in the modified version of EXSIM (Boore, 2009), stress parameter is

similar to SMSIM (Boore, 2005) which comes directly from concept of stress drop in Brune source model (Brune, 1970). Crustal shear wave velocity and crustal density are taken from the work of Radjaee et al (2010). They determined a model of the crust for the central Alborz Mountains using teleseismic receiver functions from data recorded on a temporarily network. Rupture velocity is considered to be 0.8 times of shear wave velocity. (Beresnev and Atkinson, 1999; Atkinson and Boore, 2006; Motazedian, 2006).

Table 1 Modeling parameters

Fault orientation	Strike 265˚; Dip 50˚
Fault dimensions along strike and dip	44 by 20 km
Fault depth range	3 – 18 km
Moment magnitude	7.0
Subfault dimensions	2 by 2 km
Stress parameter	120 bars
Number of subfaults	220
Q (f)	$87f^{1.147}$
Geometrical spreading	R^{-1}, $R \leq 70$ km R^{-2}, $70 < R \leq 150$ km $R^{-.5}$, $R > 150$
Windowing function	Saragoni-Hart
Kappa factor (High-cut filter)	0.05
Pulsing area	50%
Crustal shear-wave velocity	3.5 km/sec
Rupture velocity	0.8 × shear wave velocity
Crustal density	2.8 g/cm^3

We don't have information of slip distribution on the fault; therefore we assume two asperities on the fault with combined area equal to 22% of the total area of the fault (Somerville et al, 1999; Irikura et al, 2004; Irikura and Miyake, 2010). Location of asperities and rupture starting point are decided following "recipe" (Irikura et al, 2004; Irikura and Miyake, 2010). Slip rate on asperities are two times of average slip on the fault (Irikura and Miyake, 2010, Dalguer et al, 2004).

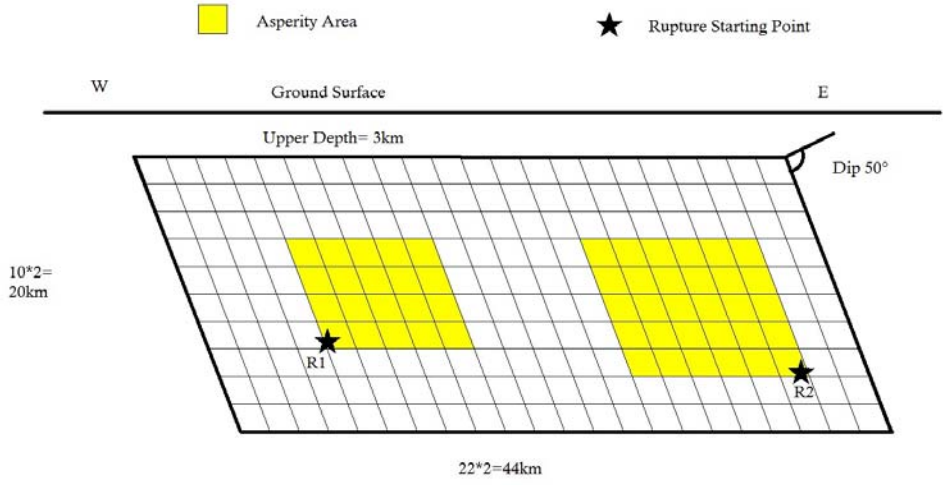

Figure 2. Geometry of the fault

In **Figure 2**, geometry of the fault, subfaults, asperity area and locations of rupture starting points are shown. This model is used to generate acceleration time histories in 836 points in Metropolitan of Tehran. These points along with projection of the fault model on ground surface are shown in **Figure 3.** Simulations are executed for generic rock sites with the average shear wave velocity of 620 m\sec in the upper 30 meters of the site. The site amplification factors employed here are those of Boore and Joyner (1997) for various typical site conditions.

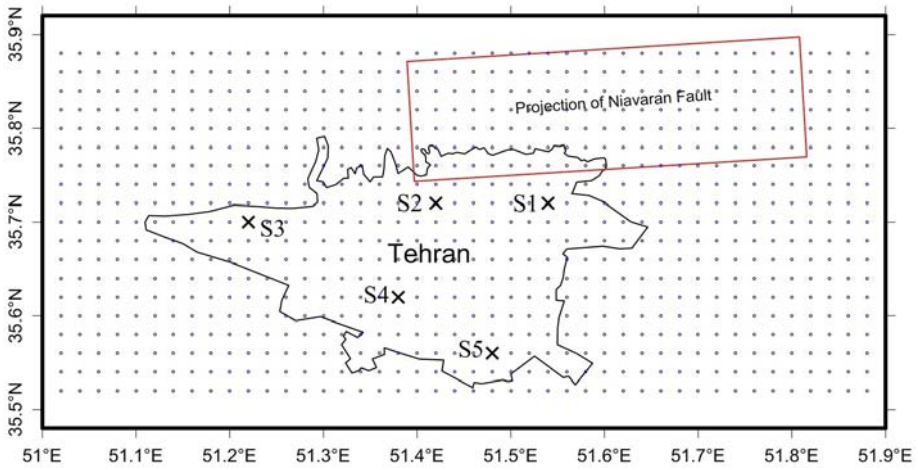

Figure 3. Simulation points in Tehran (Crosses are the sites that their acceleration time histories are shown)

a)

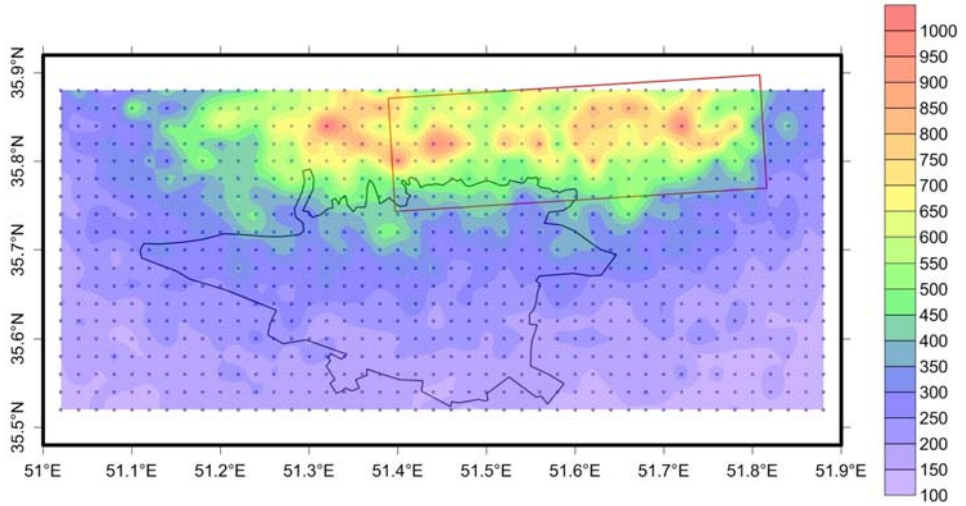

b)

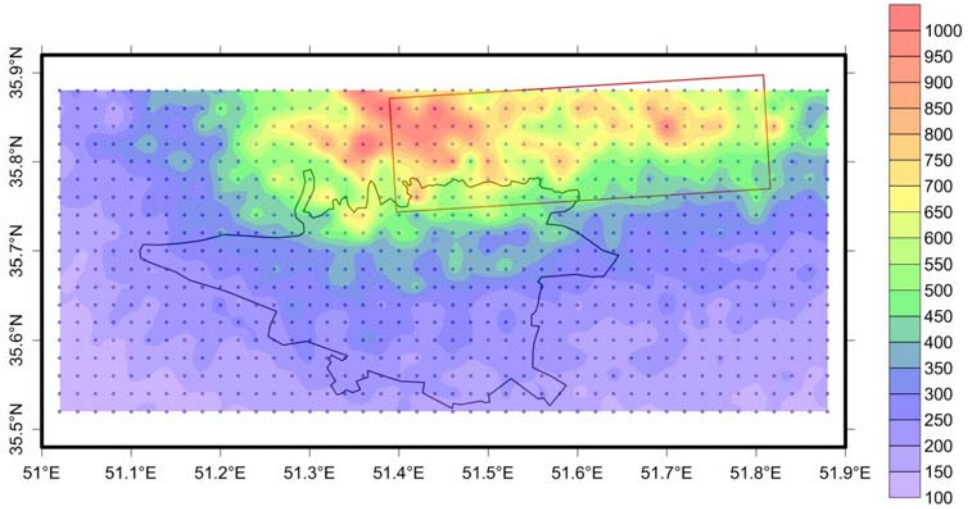

Figure 4. Shake map for PHA in Tehran for: a) Rupture starting point of R1. b) Rupture starting point of R2. (Units are in cm/sec^2)

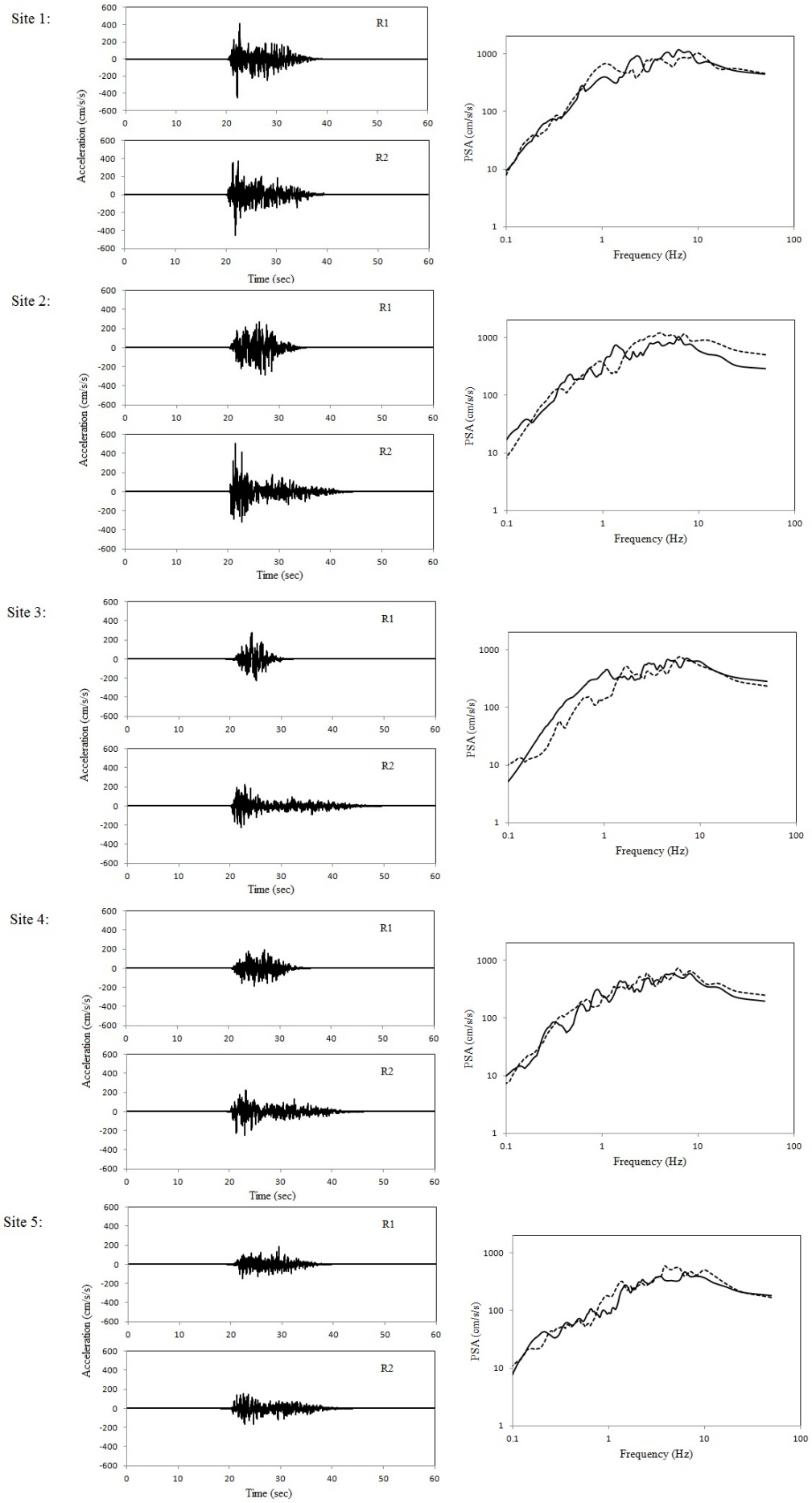

Figure 5. Acceleration time histories and their 5% damped pseudo-acceleration response spectra. For each site time histories for rupture starting point of R1 and R2 are drawn. In PSA diagram solid line is for R1 and dotted line is for R2.

Shake map of peak horizontal acceleration (PHA) from simulated time histories for two rupture starting points are shown in **Figure 4.** As it can be seen the amount of PHA in Tehran varies from 100 cm/sec^2 in south to 800 cm/sec^2 in the north of the city which proves Niavarn Fault is one of the most hazardous faults for northern Tehran while for southern Tehran the other faults like North and South Rey Faults and Parchin Fault are probably most hazardous.

In **Figure 5.** Acceleration time histories and their 5% damped pseudo-acceleration response spectra of 5 selected sites of **Figure 3** are drawn.

4. COMPARISON WITH ATTENUATION RELATIONS

Since in recent years no earthquake of target moment has happened around Tehran and thus no strong-motion recordings are available to compare the results of the simulations with actual data, we chose to draw a comparison with attenuation laws developed for Iranian plateau. Attenuation relationships estimate ground motion as a function of magnitude and distance.
Using the stochastic finite-fault model of Motazedian and Atkinson (2005) with the model parameters listed in **Table 1**, we generated random horizontal components of motion in different distances for two types of soil conditions. Soil conditions we considered here are general rock and general soil sites (Boore and Joyner, 1997). General rock and soil sites have V_{S30} =620 m/s and V_{S30} =310 m/s respectively. (V_{S30} is the time-averaged shear-wave velocity in the top 30 m of the site profile). Same asperity condition of **Figure 2.** is considered and tow more rupture nucleation points are assumed in order to produce more data. We simulated records for distances from surface projection of the fault ranging from 1 to 400. (Note, the actual distances from surface projection of the fault are as follows: 1, 2, 5, 10, 15, 20, 30, 40, 50, 60, 70, 80, 100, 120, 150, 200, 250, 300 and 400 km.) Eight lines at equally spaced azimuths spreading out from a point above the center of the top of the fault plane were defined to capture the average effect of directivity.

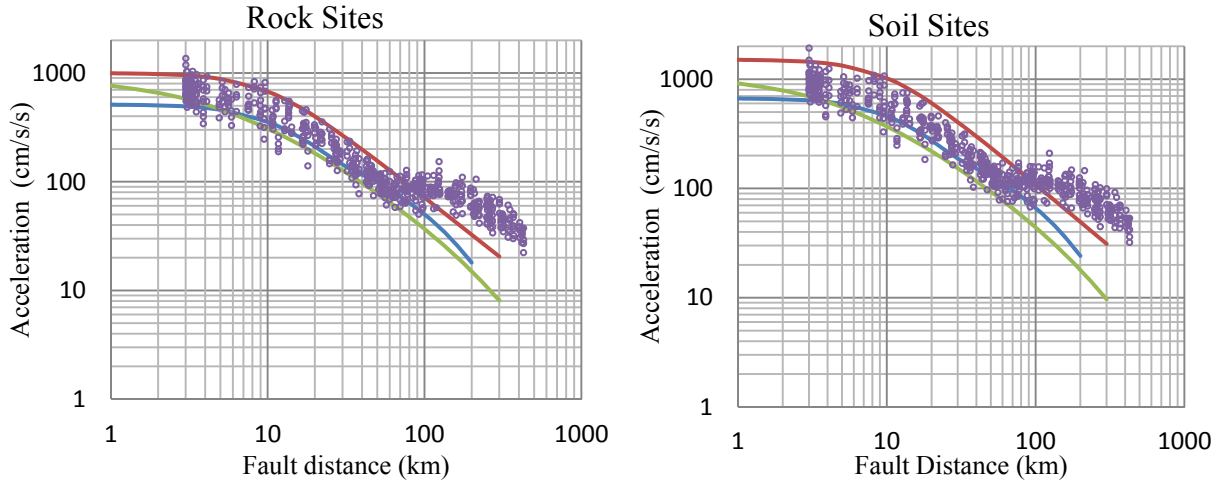

Figure 6. PHA from simulations versus closest distance to the rupture of the fault (dots) in comparison with three attenuation models; first: Sinaeian et al, (green line), second: Zaferani et al, (blue line), third: Nowroozi (red line)

Figure 6. plots PHA from simulations versus closest distance to the rupture on the fault in comparison with three empirical attenuation models. First: Sinaeian et al, (2007), second: Zaferani et al, (2008) and third: Nowroozi (2005). Curves are drawn for two types of soil profile with V_{S30}=620 m/s and V_{S30}=310 m/s and for every soil profile total number of 608 simulations have done (19 distances × 8 azimuthally equal lines × 4 rupture starting points). It should be noted here that our definition of distance here is M4 of the distances defined by Joyner and Boore (1988).

As can be seen in the **Figure 6**, our simulations show a general agreement with all curves at distances up to 70 kilometres (Which is used in this study). At distances further than 70 kilometres our simulations show bigger amounts compared to all of the attenuation models. This is mostly because of the shape of geometrical spreading which is almost constant in distances from 70 to 150 km. Although this type of geometrical spreading is widely used in all regions of the world but more researches similar to Atkinson (2004) for finding a better function for geometric spreading should be done in Iran.

5. CONCLUTIONS

By finite fault modeling, acceleration time histories were predicted at 836 points in metropolitan of Tehran to draw PHA shake map of Tehran for generic rock sites. "Recipe" for predicting strong ground motion from crustal earthquake scenarios was followed to characterize source model of Niavarn Fault. PHA from simulations varies from 100 cm/sec^2 in southern part of the city to 800 cm/sec^2 for Northern part. We also compared results of our simulations in different distances with attenuation relationships. PHA of our finite fault simulations are in general agreement in distances up to 70 kilometers. For better agreement in wider range of distance coefficients of geometrical spreading should be modified.

REFERENCES

Abbassi, M., R. and Farbod, Y. (2009). Faulting and folding in quaternery deposits of Tehran's piedmont (Iran). *Journal of Asian earth sciences*. **34:** 522-531.

Atkinson, G. (2004). Empirical Attenuation of Ground Motion Spectral Amplitudes in Southeastern Canada and The Northeastern United States. *Bulletin of the Seismological Society of America.* **94:** 1079–1095.

Atkinson, G. M. and Boore, D. M. (2006). Earthquake ground motion prediction equations for Eastern North America, *Bulletin of the Seismological Society of America*. **96:** 2181–2205.

Berberian, M., Qorashi, M., Arzhangravesh, B. and Mohajer-Ashtiani, A. (1983). Recent Tectonics, Seismotectonics and Earthquake-Fault Hazard Study in the Greater at Tehran Region. Geological Survey of Iran, Iran. (in Persian).

Berberian, M., Yeats, R.S., (1999). Patterns of historical earthquake rupture in the Iranian Plateau. *Bulletin of the Seismological Society of America*. **89:** 120–139.

Beresnev, I. A. and Atkinson, G. M. (1997) Modeling finite-fault radiation from the ω^2 spectrum, *Bulletin of the Seismological Society of America*. **87:** 67-84.

Beresnev, I. A. and Atkinson, G. M. (1999). Generic finite fault model for ground-motion prediction in Eastern North America, *Bulletin of the Seismological Society of America,* **89:** 608-625.

Boore, D. M. (1983). Stochastic simulation of high-frequency ground motions based on seismological models of the radiated spectra, *Bulletin of the Seismological Society* of *Americ*a. **73:** 1865-1894.

Boore, D. M. (2003). Simulation of Ground Motion Using the Stochastic Method. *Pure and Applied Georhysics.* **160:** 635-676.

Boore, D. M. (2005). SMSIM−Fortran Programs for Simulating Ground Motions from Earthquakes: Version 2.3−A Revision of OFR 96-80- A, U.S. Geol. Surv. Open-File Report 00-509

Boore, D. M. (2009). Comparing stochastic Point-Source and Finite-Source Ground-Motion Simulations: SMSIM and EXSIM. *Bulletin of the Seismological Society* of *Americ*a. **99:** 3202-3216.

Boore, D. M. and Joyner, W. B. (1997). Site Amplification for Generic Rock Sites, *Bulletin of the Seismological Society of America*. **87:** 327 – 341.

Brune, J., N. (1970), Tectonic Stress and the Spectra of Seismic Shear Waves from Earthquakes. *Journal of Geophysical Research.* **75:** 4997-5009.

Dalguer, L. A., Miyake, H., And Irikura, K. (2004), Characterization of dynamic asperity source models for simulating strong ground motions, *Proceedings of the 13th World Conference on Earthquake Engineering*. No. 3286.

Hartzell, S. (1978). Earthquake aftershocks as Green's functions, *Geophysical Research letters*. **5:** 1-14.

Irikura, K., Miyake, H., Iwata. T., Kamar, K., Kawabe, H. and Dalguer, A. (2004). Recipe for Predicting Strong Ground Motions from Future Large Earthquakes. *Proceedings of the 13th World Conference on Earthquake Engineering.* No. 1371.

Irikura, K. and Miyake, H. (2010). Recipe for Predicting Strong Ground Motions from Crustal Earthquake Scenarios. *Pure and Applied Georhysics.* **186:** 85-104.

Joyner, W. B., Boore, D. M. (1988) Measurement, characterization, and prediction of strong ground motion, *Proceedings of Earthquake Engineering and Soil Dynamics II*.

Motazedian, D. (2006) Region-specific key seismic parameters for earthquakes in Northern Iran, *Bulletin of the Seismological Society of America*. **96:** 1383–1395.

Motazedian, D., and Atkinson, G. M. (2005). Stochastic Finite-Fault Modeling Based on a Dynamic Corner Frequency, *Bulletin of the Seismological Society of America*. **95:** 995-1010.

Nowroozi, A. (2005). Attenuation relations for peak horizontal and vertical accelerations of earthquake ground motion in Iran: a preliminary analysis. *Journal of Seismology and Earthquake Engineering.* **7:** 109−27.

Radjaee, A., Rham, D., Mokhtari, M., Tatar, M., Priestley, K. and Hatzfeld, D. (2010) Variation of Moho Depth in the Central Part of Albprz Mountains, Northern Iran. *Geophysical Journal International.* **181:** 173-184.

Sinaiean, F., Zare, M., Fukushima, Y. (2007). A study on the empirical PGA attenuation relationships in Iran. *Proceedings of the 5th international conference on seismology and earthquake engineering.*

Somerville, P., Irikura, K., Graves, R., Sawada, S., Wald, D., Abrahamson, N., Iwasaki, Y., Kagawa, T., Smith, N., And Kowada, A. (1999). Characterizing Earthquake Slip Models For The Prediction Of Strong Ground Motion, *Seismolgical Research Letters.* **70:** 59–80.

Tchalenko, J.S., Berberian, M., Iranmanesh, H., Baily, M. and Arsovsky, M.(1974). Tectonic framework of the Tehran region, *Geological Survey of Iran,* **Rep. 29:** 7-46.

Wells, D. L. and Coppersmith, K. J. (1994). New empirical relationships among magnitude, rupture length, rupture width, rupture area and surface displacement *Bulletin of the Seismological Society of America*. **84:** 974–1002.

Zafarani, Z., Mousavi, M., Noorzad, A., Ansari, A. (2008) Calibration of the specific barrier model to Iranian plateau earthquakes and development of physically based attenuation relationships for Iran. *Soil Dynamics and Earthquake Engineering.* **28:** 550–576.